High Power, Compact Picosecond Pulse Compression Based on Concave-Convex Cavity

Zhenwen Huang(黄振文)[1,3], Pinbin Li(李聘滨)[2,3], Xiaowei Xing(邢笑伟)[1,3], Qi Liu(刘齐)[1,3], Kejian Wang(王柯俭)[2,3], Wenjun Liu(刘文军)[1,5*], Hao Teng(滕浩)[3,4,6*], Jiangfeng Zhu(朱江峰)[2], and Zhiyi Wei(魏志义)[3,4,6*]

[1]*State Key Laboratory of Information Photonics and Optical Communications, School of Science, Beijing University of Posts and Telecommunications, Beijing 100876, China*
[2]*School of Optoelectronic Engineering, Xidian University, Xi'an 710071, China*
[3]*Beijing National Laboratory for Condensed Matter Physics, Institute of Physics Chinese Academy of Sciences, Beijing 100190, China*
[4]*School of Physical Sciences, University of Chinese Academy of Sciences, Beijing 100049, China*
[5]*Beijing Laser Creation Optoelectronics Technology Company Limited, Beijing 101400, China*
[6]*Songshan Lake Materials Laboratory, Dongguan 523808, China*

(Received 8 January 2025; accepted manuscript online 14 February 2025)

By combining a concave-convex multi-pass cavity with solid-state nonlinear media for spectral broadening and a post-compression grating setup, we generated femtosecond pulses with high peak power density. Compared to the other traditional pulse compression technologies, the configuration is very compact with large tolerance for beam direction and spot size. The pulses with an average power of 80 W, a pulse width of 10.7 ps, and a repetition rate of 500 kHz are compressed to 842 fs with the configuration, and the compressed pulse duration approaches the Fourier transform limited pulse duration of 707 fs.

DOI: 10.1088/0256-307X/42/2/024203 CSTR: 32039.14.0256-307X.42.2.024203

1. Introduction. Nonlinear pulse compression is a critical technology in frontier science and industrial application fields, such as high-order harmonic generation, inertial confinement fusion and precision machining, which has potential to narrow the ultrafast laser pulses near the gain bandwidth limit of their gain media. Over the past two decades, the use of few-cycle pulses produced by Ti:Sapphire lasers[1–5] had enabled unprecedented levels of spatiotemporal resolution in the attosecond domain. In addition, precise control of the energy and frequency of few-cycle pulses can be used to achieve directed heat treatment and activation of fusion materials, as well as modification of material surfaces. Despite their potential, these applications impose stringent demands on driving lasers, typically requiring sources with kilowatt-level average power and sub-picosecond pulse durations. For many desktop high-power lasers,[4–10] the main challenge now is how to efficiently compress the high-power ultrashort pulses,[11,12] generated by the laser sources to the few-cycle level, which aim to achieve hundreds of watts and millijoule-scale pulse outputs. To handle these challenges, researchers have proposed post-pulse compression techniques,[13,14] which are based on the Fourier-transform-limited (FTL) pulse principle and the generation of short pulses relies on spectra broadening.

In the field of spectral broadening, pulse compression schemes can be broadly classified into two main categories: multi-pass structures and single-pass structures. Single-pass structures, such as hollow-core fibers (HCFs) and multiple plate continuum schemes, face distinct challenges. For instance, HCFs require water cooling to avoid thermal damage under high power conditions, posing challenges in terms of beam pointing stability and manufacturing. On the other hand, multiple plate continuum schemes offer enhanced conversion efficiency and stability, but face issues with non-uniform spectral broadening and the need for precise adjustments to prevent self-focusing effects. In contrast, multi-pass structures like multi-pass cells (MPCs) stand out for their superior power, efficiency, and stability.

MPCs are capable of handling kilowatt-level average powers[15] and single-pulse energies in the hundreds of millijoules,[16,17] extending even into the few-cycle temporal domain.[18–20] With advanced coating technology, nearly lossless compression can be achieved. In recent years, numerous works have reported the generation of few-cycle pulses using gas-filled MPCs, typically employing closed cells filled with nonlinear gases such as argon (Ar),[21–23] krypton (Kr),[24,25] or mixed gases.[26] These lasers can reach hundreds of megawatts of peak power, efficiently traversing the cavity and achieving significant pulse compression ratios. Furthermore, research on multiple plate continuum, large-aperture MPC compression systems has yielded outputs sub-10 fs and gigawatt (GW,

*Corresponding author. Email: jungliu@bupt.edu.cn; hteng@iphy.ac.cn; zywei@iphy.ac.cn
© 2025 Chinese Physical Society and IOP Publishing Ltd. All rights, including for text and data mining, AI training, and similar technologies, are reserved.

10^9 W) levels. In a groundbreaking study conducted in 2023, Viotti and colleagues[27] utilized a two-stage MPC to achieve a remarkable hundredfold in pulse duration, ultimately yielding an output pulse with a Full Width at Half Maxima (FWHM) of 8.2 fs. Additionally, the combination of MPCs with HCFs or other spectral broadening devices has shown promising results in meeting these demanding requirements. However, the conventional approach of cascading MPC stages is often hindered by its large physical footprint and cost inefficiency, leading to limited adoption of setups with three or more stages. To address the demand for high power and ultra-narrow pulse width within a compact experimental setup, innovative MPCs designs have emerged, which include plano-concave cavities,[28] concave-convex cavities,[29] and bowtie cavities.[30] In this work, the intrinsic modes within the cavity and the spot sizes on the mirror surfaces were all recalculated, meanwhile, the concave-convex lens set for mode matching was also adjusted. Additionally, one fused silica block with a thickness of 15 mm and another with 20 mm were inserted into the cavity for spectral broadening as solid nonlinear media. In this configuration, the length of the cavity was shortened to 114 mm, approximately one-third of the length of a traditional double-concave cavity. A comparison between the double-concave cavity and the concave-convex cavity is illustrated in Fig. 1, where the middle line indicates the focal plane of the double-concave cavity.

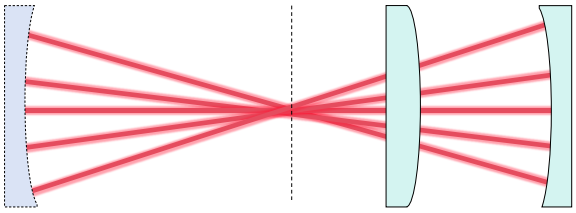

Fig. 1. Comparsion of beam propagation in double-concave and the concave-convex cavity designs.

2. Experimental Principle and Numerical Simulation. Analyzing the concave-convex cavity of a MPC in terms of stable resonant cavity behavior reveals that, once the parameters and spacing of the concave-convex cavity mirrors are fixed, the self-reproducing modes within the cavity are also determined accordingly. The positions and sizes of the laser spots on various points of the cavity mirrors can be deduced based on the eigenmodes. This holds great importance for nonlinear spectral broadening via Self-Phase Modulation (SPM) and the calculation of peak power density on the MPC cavity mirrors. We calculated the eigenmodes using the ABCD matrix method.

For the concave-convex cavity configuration, the transfer matrix for each pass was given by the following formula:

$$Q_{\mathrm{cv}} = \begin{pmatrix} 1 & 0 \\ -\frac{2}{R_{\mathrm{c}}} & 1 \end{pmatrix} \begin{pmatrix} 1 & L \\ 0 & 1 \end{pmatrix} \begin{pmatrix} 1 & 0 \\ -\frac{2}{R_{\mathrm{v}}} & 1 \end{pmatrix} \begin{pmatrix} 1 & L \\ 0 & 1 \end{pmatrix}. \quad (1)$$

Here, Q_{cv} represents the transfer matrix for the concave-convex MPC cavity. R_{c} and R_{v} denote the curvature radii of the convex reflective mirror and the concave reflective mirror, respectively, while L stands for the cavity length.

For the eigenmodes q_i to satisfy the condition of self-reproduction, which must fulfill the following equation:

$$q_i = \frac{Aq_i + B}{Cq_i + D}. \quad (2)$$

Here, A, B, C, D are elements of matrix Q_{cv}.

From the formulas for calculating the beam waist w_i and the Rayleigh length z_0 in a resonant cavity:

$$w_i = \sqrt{\frac{\lambda z_0}{\pi}}, \quad (3)$$

$$z_0^2 = \frac{L(-R_{\mathrm{c}} - L)(R_{\mathrm{v}} - L)(R_{\mathrm{c}} - R_{\mathrm{v}} - L)}{(R_{\mathrm{c}} - R_{\mathrm{v}} - 2L)^2}, \quad (4)$$

and the formula for calculating the radius of the light spots on the mirror surface:

$$w(z) = w_i \sqrt{1 + \frac{z^2}{z_0^2}}. \quad (5)$$

Through calculations, it's straightforward to obtain the spot radii on the concave mirror (with a radius of curvature of 200 mm) and the convex mirror (with a radius of curvature of −250 mm) as $w_{\mathrm{c}} = 340.348\,\mu$m and $w_{\mathrm{v}} = 185.438\,\mu$m, respectively. Based on the laser parameters, the peak power density within the cavity is calculated to be 1.4×10^{10} W·cm^{-2}, which is less than the damage threshold of the cavity mirrors (10^{11}–10^{12} W·cm^{-2}). Additionally, the peak energy density within the cavity is 0.15 J·cm^{-2}, which is lower than the ionization threshold of fused silica (5.335 J·cm^{-2}).

To achieve precise mode matching, the numerical method was used to simulate the size of the laser beam spot size. By directing the beam through a lens set, the output mode of the laser source was matched to the eigenmode of the concave-convex resonant cavity, ensuring substantial alignment. Fig. 2 shows the simulated beam spot radii ($w_{\mathrm{cs}} = 332.831\,\mu$m and $w_{\mathrm{vs}} = 183.373\,\mu$m) at 330 mm from the lens set closely matching the eigenmode requirements of the cavity. This alignment satisfies the condition of mode self-reproduction within the cavity, thereby guaranteeing high stability of the concave-convex MPC under high-energy conditions.

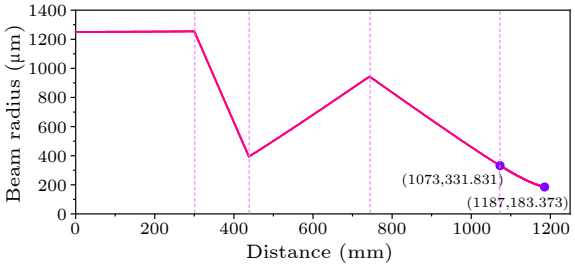

Fig. 2. Utilize the numerical simulation method to match patterns in the simulated model of concave-convex MPC. The vertical purple dotted lines indicate the positions of optical elements, with the two annotated points specifically denoting the locations of the concave and convex mirrors. The ordinate represents the radius of the laser spots on the mirror surface.

3. Instrumental Facilities and Result Discussion. The objective of this work is to investigate the potential of spectral broadening using a concave-convex cavity with

high-power picosecond pulse lasers. Figure 3 presents a schematic diagram of the concave-convex cavity setup, utilizing a 10 ps laser with a central wavelength of 1064 nm. The laser delivers an average power of 80 W, features a pulse duration of 10.7 ps and a repetition rate of 500 kHz. The resulting output spectrum, shown in Fig. 4(a), exhibits an FWHM of 0.24 nm.

The output pulses from the picosecond laser were mode-matched through a lens set and directed into a concave-convex cavity via a rectangular mirror with dimensions of $5 \times 10 \times 3\,\text{mm}^3$. Within the cavity, the pulse completes 23 round trips, undergoing spectral broadening due to the self-phase modulation effect during each pass through the nonlinear medium. The broadened spectrum, measured with a spectrometer (YOKOGAWA, AQ6370C), is compared to the initial spectrum in Fig. 4(c). Then, the laser was reflected by the same rectangular mirror and enters a grating compressor module which comprises two transmission gratings with 1000 line/mm, spaced 550 mm apart. The laser beam entered the gratings at a Littrow angle of 32.1° and passes through four times, resulting in a second-order dispersion of $-3.87\times10^6\,\text{fs}^2$ and a third-order dispersion of $11.746\times10^6\,\text{fs}^3$. Upon exiting the compressor module, the positive second and third-order dispersion accumulated within the cavity were compensated, compressing the pulse to the femtosecond scale. Autocorrelation trace of pulse measurements (APE, pulse check 50) indicates that the output pulse closely approaches the FTL, as depicted in Fig. 4(d).

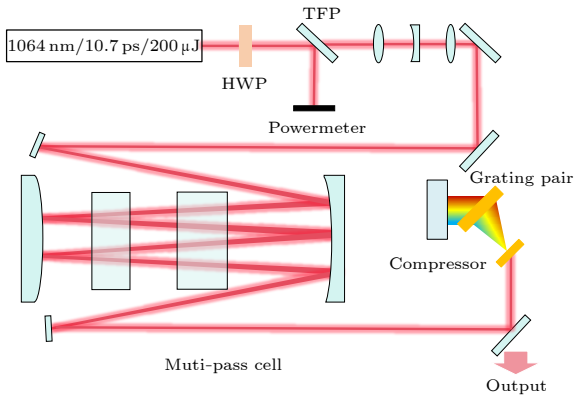

Fig. 3. Schematic diagram of the concave-convex MPC device.

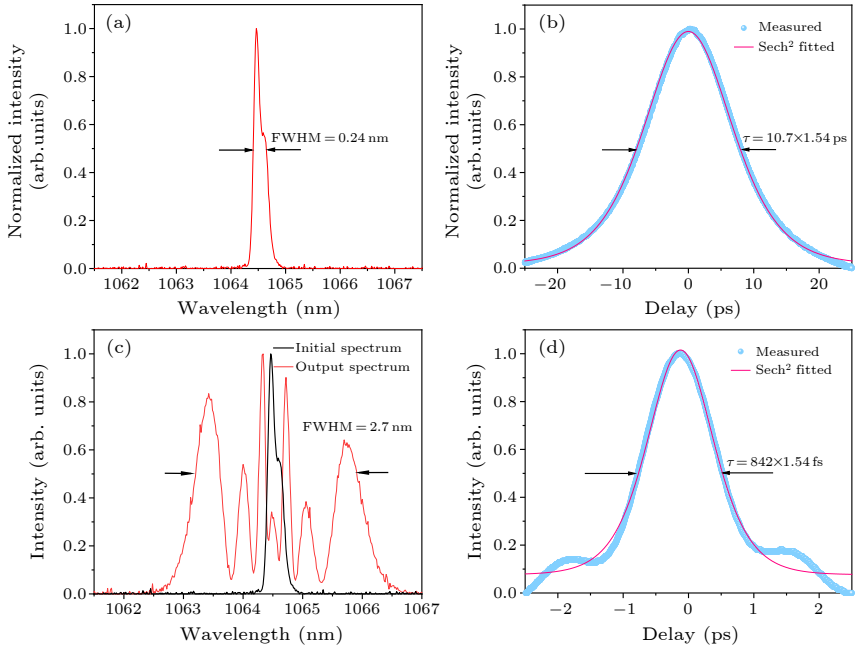

Fig. 4. Characterization of pulses compressed by the concave-convex MPC. (a) Initial spectra of picosecond laser; (b) initial pulse autocorrelation trace of picosecond laser; (c) comparison of input and output spectra; (d) output autocorrelation trace of pulse.

Simultaneously, the beam quality of the output from a picosecond laser and the beam quality after the concave-convex MPC device were measured and compared using an M^2 Beam Quality Analyzer (Ophir, Beamsquared® SP920). The measurement results are presented in Fig. 5, showing that the beam quality changed from $M^2_{xy} = 1.368 \times 1.305$ to $M^2_{xy} = 1.430 \times 1.201$. The slight deterioration in M^2 values can be attributed to the attenuation elements used prior to the measurement.

Table 1 presents a selection of representative studies in single-stage MPC pulse compression from recent years for comparison. As shown, single-stage MPC configurations targeting high peak power densities ($> 10^{10}\,\text{W}\cdot\text{cm}^{-2}$) generally employ extended cavity lengths and larger intrinsic mode sizes within the cavity to mitigate risks of mirror damage and ionization. For example, in Ref. [17], Pfaff *et al.* compressed pulses with an individual pulse energy of 200 mJ within a 10 m vacuum chamber housing concave mirrors, using 800 mbar of Ar as the nonlinear medium. However, excessively long cavity lengths can lead

to elevated costs and reduced pointing stability. In comparison to the picosecond compression setups reported in Refs. [28], [32], and [35], the approach in this work achieved femtosecond laser output at higher peak power densities, while offering benefits in reduced cavity length, thereby enhancing system stability and lowering construction costs. Based on the work of Victor *et al.*,[36] this paper demonstrates a cost-effective, high-stability, high-power picosecond post-compression setup with a cavity length of only 114 mm, achieving an average power output of 60.8 W and a compression ratio of 13. The main reason for the power decrease is optical loss. Assuming the cavity mirrors reflectivity and FS transmittance are 99.9%, the efficiency of the MPC is $0.999^{138} = 87.1\%$. Therefore, the efficiency is closely related to the coating of optical components. Subsequently, custom FS with a transmittance greater than 99.9% can be used to improve efficiency.

Table 1. Comparison of nonlinear pulse compression technology in single-stage MPC.

P_{in} (W)	P_{out} (W)	τ_{in} (fs)	I_{peak} (W·cm^{-2})	τ_{out} (fs)	L (mm)	Refs.
40	36.7	220	2.2×10^{11}	27	1340	[31]
230	117	11300	1.9×10^{9}	1420	550	[32]
780	–	461	3.5×10^{10}	32	10^4	[17]
34	30	300	–	30	500	[33]
1.6	–	670	5.9×10^{10}	133	615	[29]
112	–	1240	2.8×10^{11}	39	385	[34]
1.65	1.23	12500	2.6×10^{9}	601	500	[35]
100	44.2	10700	1.2×10^{10}	483	150	[28]
15	13.9	260	2.6×10^{11}	56	283	[36]
15	13.6	260	1.0×10^{11}	50	114	[36]
80	**60.8**	**10700**	$\mathbf{1.4 \times 10^{10}}$	**842**	**114**	**This work**

Notes: P_{in}: the average power of input; P_{out}: the average power of output; τ_{in}: pulse duration of input; I_{peak}: peak energy density; τ_{out}: pulse duration of output; L: the length of the cavity.

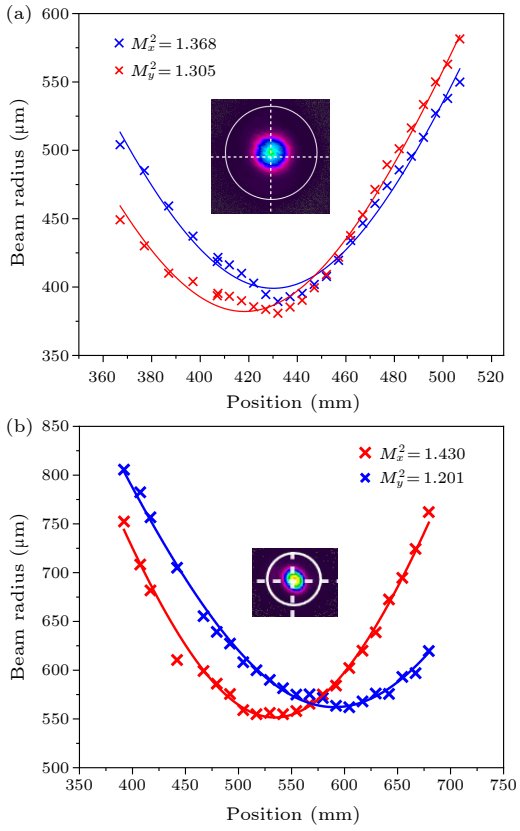

Fig. 5. (a) Initial M^2 plot of the laser; (b) M^2 after broadening and compression via concave-convex MPC.

4. Conclusion. In summary, a nonlinear pulse compression setup based on a concave-convex MPC combined with solid nonlinear media had been successfully implemented. The MPC structure consists of a concave mirror and a convex mirror, incorporating 15 mm and 20 mm fused silica blocks as solid nonlinear media to achieve spectral broadening. Silica blocks have been positioned within the concave-convex cavity, which has a total length of 114 mm. Following spectral broadening, pulse compression was achieved through dispersion compensation using a pair of transmission gratings. A laser with an average power of 80 W at a repetition rate of 500 kHz, and an initial pulse width of 10.7 ps was injected into the concave-convex MPC cavity. After 46 passes through the fused silica nonlinear media, the spectral FWHM broadens from 0.24 nm to 2.7 nm. A pair of 1000 line/mm transmission gratings was used for dispersion compensation, compressing the pulse duration from 10.7 ps to 842 fs, achieving a compression ratio of 13. The MPC output power was 71.5 W, which decreased to 60.8 W after passing through the grating compressor, primarily due to grating diffraction efficiency and coating absorption. The beam quality of the laser output from the MPC cavity, characterized by $M_{xy}^2 = 1.430 \times 1.201$, remains close to the input beam quality. Experimental results demonstrate that the improved concave-convex MPC setup offers a more compact structure than traditional cavity designs, along with excellent power stability, pointing stability, and a high compression ratio. This configuration presents an approach for generating high-power femtosecond laser sources. The high-power femtosecond laser produced by this method holds promising applications across various fields, including micro-nano precision processing, high-precision medical surgery, and high-order harmonic generation.

Acknowledgements. This work was supported by the National Key Research and Development Program of China (Grant Nos. 2022YFA1604200 and

2022YFB4601101), the Beijing Municipal Commission of Science and Technology (Grant No. Z231100006623006), the Beijing Natural Science Foundation (Grant No. JQ21019), and the National Natural Science Foundation of China (Grant Nos. 12034020, 11975001, 12075034, and 12261131495).

References

[1] Nisoli M, De Silvestri S, and Svelto O 1996 *Appl. Phys. Lett.* **68** 2793
[2] Schenkel B, Biegert J, Keller U, Vozzi C, Nisoli M, Sansone G, Stagira S, De Silvestri S, and Svelto O 2003 *Opt. Lett.* **28** 1987
[3] Cavalieri A L, Goulielmakis E, Horvath B, Helml W, Schultze M, Fiess M, Pervak V, Veisz L, Yakovlev V S, Uiberacker M, and Apolonski A 2007 *New J. Phys.* **9** 242
[4] Jiang J W, Fang S B, Zhang Z Y, Zhu J F, Han H N, Chang G Q, and Wei Z Y 2020 *Chin. Phys. Lett.* **37** 054201
[5] Liu K Y, Liu Y Q, Tang Y H, Chen J C, Wang C, Liu X Y, Wang X B, Long Y B, Xu Y, Peng Y J, Lu X M, Liu Z Z, and Leng Y X 2021 *Chin. Opt. Lett.* **19** 011401
[6] Budriūnas R, Stanislauskas T, Adamonis J, Aleknavičius A, Veitas G, Gadonas D, Balickas S, Michailovas A, and Varanavičius A 2017 *Opt. Express* **25** 5797
[7] Trovatello C, Marini A, Xu X Y, Lee C, Liu F, Curreli N, Manzoni C, Conte S D, Yao K Y, Ciattoni A, Hone J, Zhu X Y, Schuck P J, and Cerullo G 2021 *Nat. Photon.* **15** 6
[8] Xu Y C, Wang Z M, Zhang F F, Yang R N, Liu X C, Song Y, Bo Y, Peng Q J, and Xu Z Y 2020 *Chin. Phys. Lett.* **37** 054203
[9] Wang H L, Dong J J, Liu H Y, Hao J J, Zhu X, and Zhang J W 2021 *Acta Photon. Sin.* **50** 0850208 (in Chinese)
[10] Cui W W, Xing X W, Chen Y Q, Xiao Y J, Ye H, and Liu W J 2023 *Chin. Phys. Lett.* **40** 024201
[11] Wang L, Wang X W, Xiao F, Wang J C, Tao W K, Zhang D W and Zhao Z X 2023 *Chin. Phys. Lett.* **40** 113201
[12] Yan S J, Xu Q Y, Hao X Y, Guo Y and Guo J 2023 *Chin. Phys. Lett.* **40** 113101
[13] Nagy T, Simon P, and Veisz L 2021 *Adv. Phys.: X* **6** 1845795
[14] Viotti A L, Seidel M, Escoto E, Rajhans S, Leemans W P, Hartl I, and Heyl C M 2022 *Optica* **9** 197
[15] Grebing C, Müller M, Buldt J, Stark H, and Limpert J 2020 *Opt. Lett.* **45** 6250
[16] Kaumanns M, Kormin D, Nubbemeyer T, Pervak V, and Karsch S 2021 *Opt. Lett.* **46** 929
[17] Pfaff Y, Barbiero G, Rampp M, Klingebiel S, Brons J, Teisset C Y, Wang H, Jung R, Jaksic J, Woldegeorgis A H, and Trunk M 2023 *Opt. Express* **31** 22740
[18] Müller M, Buldt J, Stark H, Grebing C, and Limpert J 2021 *Opt. Lett.* **46** 2678
[19] Lu C H, Witting T, Husakou A, Vrakking M J J, Kung A H, and Furch F J 2018 *Opt. Express* **26** 8941
[20] Daniault L, Cheng Z, Kaur J, Hergott J F, Réau F, Tcherbakoff O, Daher N, Délen X, Hanna M, and Lopez-Martens R 2021 *Opt. Lett.* **46** 5264
[21] Lavenu L, Natile M, Guichard F, Zaouter Y, Delen X, Hanna M, Mottay E, and Georges P 2018 *Opt. Lett.* **43** 2252
[22] Kaumanns M, Pervak V, Kormin D, Leshchenko V, Kessel A, Ueffing M, Chen Y, and Nubbemeyer T 2018 *Opt. Lett.* **43** 5877
[23] Stark H, Grebing C, Buldt J, Klenke A, and Limpert J 2022 *J. Phys.: Photon.* **4** 035001
[24] Gierschke P, Grebing C, Abdelaal M, Lenski M, Buldt J, Wang Z, Heuermann T, Mueller M, Gebhardt M, Rothhardt J, and Limpert J 2022 *Opt. Lett.* **47** 3511
[25] Karst M, Pfaller P, Klas R, Wang Z, Gierschke P, Rothhardt J, and Limpert J 2023 *Opt. Lett.* **48** 1300
[26] Eisenbach L, Wang Z, Schulte J, Heuermann T, Russbüldt P, Meyer R, Gierschke P, Lenski M, Sugiura M, Tamura K, and Limpert J 2024 *J. Phys.: Photon.* **6** 035015
[27] Viotti A L, Li C, Arisholm G, Winkelmann L, Hartl I, Heyl C M, and Seidel M 2023 *Opt. Lett.* **48** 984
[28] Li P B, Teng H, Tian W L, Huang Z W, Zhu J F, Zhong S Y, Yun C X, Liu W J, and Wei Z Y 2024 *Acta Phys. Sin.* **73** 124206 (in Chinese)
[29] Omar A, Vogel T, Hoffmann M, and Saraceno C J 2023 *Opt. Lett.* **48** 1458
[30] Schönberg A, Rajhans S, Khodakovskiy N, Escoto E, Hariton V, Hartl I, and Heyl C M 2024 *High-Brightness Sources and Light-Driven Interactions Congress paper* HTu3B.2
[31] Omar A, Hoffmann M, Galle G, Sylla F, and Saraceno C J 2024 *Opt. Express* **32** 13235
[32] Song J, Wang Z, Lv R, Wang X, Teng H, Zhu J, and Wei Z 2021 *Appl. Phys. B* **127** 50
[33] Raab A K, Seidel M, Guo C, Sytcevich I, Arisholm G, L'Huillier A, Arnold C L, and Viotti A L 2022 *Opt. Lett.* **47** 5084
[34] Seidel M, Balla P, Li C, Arisholm G, Winkelmann L, Hartl I, and Heyl C M 2022 *Ultrafast Sci.* **2022** 9754919
[35] Song J J, Wang Z H, Wang X Z, Lü R C, Teng H, Zhu J F, and Wei Z Y 2021 *Chin. Opt. Lett.* **19** 093201
[36] Hariton V, Fritsch K, Schwarz K, Kovalenko N, Figueira G, Arisholm G, and Pronin O 2023 *Opt. Express* **31** 19554